JOURNAL OF THERMOPHYSICS AND HEAT TRANSFER
Vol. 23, No. 3, July–September 2009

Thermal Modeling of Spray Cooling: Gravitational Effect on Droplet and Bubble Dynamics

R. Panneer Selvam,* Matthew T. Hamilton,† and Joseph E. Johnston III‡
University of Arkansas, Fayetteville, Arkansas 72701
and
Eric A. Silk§
NASA Goddard Space Flight Center, Greenbelt, Maryland 20771

DOI: 10.2514/1.36718

As the need for thermal management of high-power density electronic systems on space-based platforms (i.e., laser diode arrays, multichip modules, etc.) grows, interest in spray cooling as a thermal management solution is also increasing. The present study investigates numerically the effects of microgravity and macrogravity on spray cooling heat transfer as well as the effect of droplet impact on vapor bubble growth and development in a liquid film at the heater surface. A two-dimensional, multiphase flow computer model has been developed that includes the effects of surface tension, viscosity, phase change, and gravity. The liquid–vapor interface is modeled using the level set method. Initially, vapor bubble growth is simulated as pool boiling in the film's macroregion (1 to 10 mm normal to the heated wall) for purposes of model verification. Then, bubble merger in a thin film is simulated under microgravity and macrogravity conditions. Finally, droplet impingement is included in the thin-film model, and gravitational effects on the transport properties are discussed. For the thin-film bubble merger and droplet impingement simulation studies, the liquid film adjacent to the heated wall has been approximated as 70 μm thick. Wall heat transfer during droplet impingement was computed in terms of the nondimensional Nusselt number for gravitational constants ranging from 0.0001 to 2g. Computed Nusselt number versus time is presented and explained using spatial velocity vector diagrams for each simulation case. All of the computational studies were performed using FC-72 as the simulated fluid.

Nomenclature

Bo	=	Bond number, $g(\rho_1 - \rho_v)\, l_r^2/\sigma$
c_p	=	specific heat at constant pressure, kJ/kg K
Fr	=	Froude number, $u_r/\sqrt{(g l_r)}$
g	=	gravity vector, m/s^2
H	=	step function
h	=	grid spacing
h_{fg}	=	enthalpy of vaporization, kJ/kg
Ja	=	Jakob number, $c_{\mathrm{pl}}\Delta T/h_{\mathrm{fg}}$
k	=	thermal conductivity, W/m K
l_r	=	characteristic length, $\sqrt{\sigma/g(\rho_l - \rho_v)}$
$\dot{m}''$	=	mass flux vector
Nu	=	Nusselt number
$\overline{Nu}$	=	time-averaged Nusselt number
P	=	pressure, N/m^2
Pe	=	Peclet number, $\rho_l u_r l_r c_{\mathrm{pl}}/k_l$
Pr	=	Prandtl number, $c_{\mathrm{pl}}\mu_l/k_l$
$\dot{q}''$	=	heat flux, W/cm^2
Re	=	Reynolds number, $\rho_l u_r l_r/\mu_l$
T	=	temperature, K
T^*	=	dimensionless temperature
t	=	time, s
t_r	=	characteristic time
$\mathbf{u}$	=	velocity vector, u, v
$\mathbf{u}_{\mathrm{int}}$	=	interface velocity vector
u_r	=	characteristic velocity
We	=	Weber number, $\rho_l u_r^2 l_r/\sigma$
α	=	thermal diffusivity, m^2/s
ΔT_w	=	wall superheat temperature, T_w-T_{sat}
κ	=	interfacial curvature
μ	=	dynamic viscosity, N s/m^2
ρ	=	density, kg/m^3
σ	=	surface tension, N/m
φ	=	level set function

Subscripts

int	=	interface
l	=	liquid
sat	=	saturation
v	=	vapor
w	=	wall

I. Introduction

SPRAY cooling has been a topic of study in quenching and thermal management since the mid-1970s [1]. It is a heat transfer technique that has been used in industry for many years (e.g., foundry metal quenching) and has a proven capability of high heat flux heat removal (upwards of 100 W/cm^2 with fluorinerts [2] and 1000 W/cm^2 using water [3]). Several experiments dedicated to gaining a better understanding of the spray cooling process have been conducted in recent years [2–7]. However, despite its frequent use and experimental background, a theoretical understanding of spray cooling phenomena and the heat transfer mechanisms associated with it has yet to be attained. This is due to the highly complex interactions in the thin liquid film resulting from liquid droplet impact at the liquid–vapor interface and phase change in the liquid film (shown in Fig. 1). Nonetheless, understanding the fundamental transport processes that occur in spray cooling is of significant importance for improving future spray cooling systems in both terrestrial and extraterrestrial environments.

Received 18 January 2008; revision received 4 August 2008; accepted for publication 5 February 2009.

*Professor, Civil Engineering, Bell Engineering Center 4190; rps@uark.edu.
†Research Assistant, Microelectronics-Photonics.
‡Research Assistant, Microelectronics-Photonics.
§Thermal Engineer, Thermal Engineering Technology Development Group.

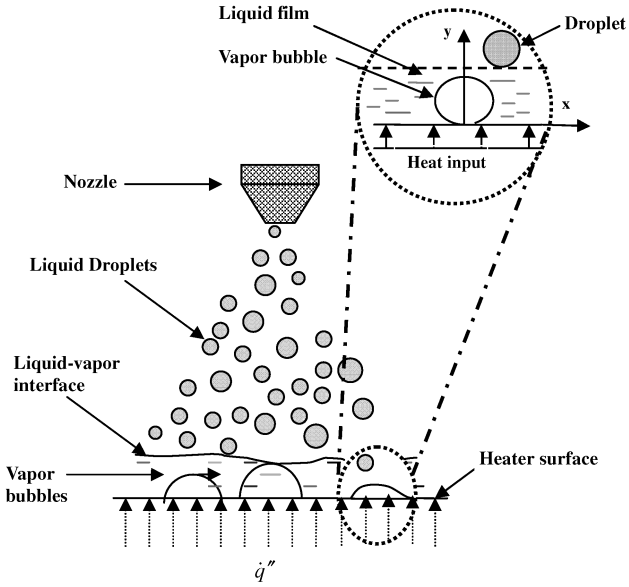

Fig. 1 Spray cooling heat transfer process schematic.

Each of the aforementioned aspects (phase change, droplet impact, bubble growth, and bulk fluid momentum) has been investigated individually. However, a comprehensive study of their intercoupled effect on the overall heat transfer has yet to be performed. Because of the nonlinear nature of the transport mechanisms in the multiphase spray cooling process (and most multiphase systems in general), there are three techniques available for investigating and determining the effects of these phenomena on spray cooling heat flux: direct experimentation, visualization, and computer modeling. The current work uses a computer modeling approach, examining single bubble and droplet interactions in the liquid film region. Although this work is not intended to provide a comprehensive solution at this time, it is aimed at gaining insight regarding the heat transfer mechanisms associated with the spray cooling process. Examination of heat flux variation in terms of the nondimensional Nusselt number is the primary method used to observe the simulated heat transfer process throughout this study.

A detailed review of the current literature on computer modeling of spray cooling and methods to solve multiphase flow problems is presented in Selvam et al. [8–11]. The studies by Selvam and Ponnappan [12] and Selvam et al. [8–11] concluded that computer modeling of nucleate boiling in a thin liquid film (approximately 70 μm) experiencing droplet impingement could provide insights that may be used to design future spray cooling test platforms. In the study by Pautsch et al. [13], a variation of the liquid film thickness under the spray region was observed. These variations in liquid film thickness ranged from 42 to 162 μm under the spray region with a maximum thickness of 396 μm in the corners of the heater surface (the heater was fabricated as a serpentine resistor in thin-film ITO). In the present study, a film thickness of 73.6 μm was simulated, which corresponds to the film thickness directly under the spray as reported in the study by Pautsch et al. [13]. Previous computational efforts detailing the transient wall heat transfer associated with the growth of a vapor bubble in a thin liquid film were reported by Selvam et al. [8]. Extended studies of this simplified problem emphasized heat transfer due to bubble growth and bursting [9] as well as the effects of droplet impingement on growing bubbles [10]. The authors determined that a thin liquid film experiencing droplet impingement produced high heat transfer due to transient conduction associated with the bubble burst process.

Dhir et al. [14] and Qiu and Dhir [15] investigated the effects of microgravity on nucleate pool boiling. Dhir et al. [14] reported that bubbles grown in a reduced gravity environment grew larger and had correspondingly longer growth periods. The authors also reported that the bubbles grew in the shape of oblong spheres. In the study by Dhir et al. [14], bubble liftoff diameters reported for 1.0 and 0.0001g were 2.3 and 210 mm, respectively. Hunnell et al. [16] performed experiments investigating gravitational effects on spray cooling by varying the spray/heater orientation relative to the gravity vector in 1.0g. In the study, the authors determined that little difference was apparent between the vertical (gravity) and horizontal (simulated microgravity) orientations. They do suggest, however, that the horizontal spray configuration cannot adequately simulate reduced gravity. In the thin-film bubble growth study by Rowden et al. [7], a computer model was developed for varying gravitational constants. The computer model, which simulated a 44 $-$ μm-thick liquid film, found no significant differences in heat flux with varying gravitational constants between 0.1 and 1.0g. The present study extends the initial investigation by Rowden et al. [7] by investigating bubble growth in the liquid film under varying gravitational constants. The effect of gravitational variations on heat transfer phenomena in spray cooling is a prime consideration for determining the feasibility for application of spray cooling systems in extraterrestrial environments. To determine the mechanisms governing heat transfer in microgravity environments, a larger simulation was computed using film thickness as a varying parameter.

II. Numerical Formulation for Multiphase Flow Using Level Set Method

A review of numerical modeling techniques applied to multiphase flows can be found in Selvam et al. [8–11]. In the present study, bubble dynamics are modeled using the level set method for two-phase flow model introduced by Sussman et al. [17]. This model was initially modified and used by Son and Dhir [18] and later by Son et al. [19] for modeling vapor bubble growth due to phase change. In the work by Son and Dhir [18], the phases are defined at a certain distance relative to the liquid–vapor interface via the function φ, which can be positive or negative. A positive sign is used for the liquid phase and a negative sign for the vapor phase. For more information on the level set method and its applications, see the works of Sethian [20] and/or Osher and Fedikiw [21]. These texts provide extensive examples of applications that use the level set method in various areas of science and engineering.

A. Governing Equations

In the present model, the fluid properties (i.e., density, viscosity, and thermal conductivity) are held constant for both phases. The flow is assumed to be incompressible. The Navier–Stokes equations used are as follows:

$$\rho(\partial_t \mathbf{u} + \mathbf{u}\nabla\mathbf{u}) = -\nabla p + \rho g - \sigma\kappa\nabla H + \nabla\mu\nabla\mathbf{u} + \nabla\mu\nabla\mathbf{u}^T \quad (1)$$

$$\rho c_{\text{pl}}(\partial_t T + \mathbf{u}\nabla T) = \nabla k\nabla T \quad \text{for } H > 0$$
$$\text{and} \quad T = T_{\text{sat}}(p_v) \quad \text{for } H = 0 \quad (2)$$

$$\nabla\mathbf{u} = \mathbf{m}\nabla_\rho/\rho^2 \quad (3)$$

where

$$\rho = \rho_v + (\rho_l - \rho_v)H \quad (4)$$

These governing equations incorporate the effects of surface tension, gravity, and phase change at the interface. The value of μ and k are calculated using a relation similar to Eq. (4). The value H is determined as

$$H = 1 \quad \text{if } \varphi \geq 1.5h \quad (5)$$

$$= 0.5 + \varphi/(3h) + \sin[2\pi\varphi/(3h)]/(2\pi) \quad \text{if } |\varphi| \leq 1.5h \quad (6)$$

$$= 0 \quad \text{if } \varphi \leq -1.5h \quad (7)$$

The variable h is the grid spacing. Equation (5) implies that the interface separating the two phases is represented by a transition region of finite thickness. The volume source term included in the continuity equation [Eq. (3)] due to liquid–vapor phase change is derived from the conditions of mass continuity and an energy balance at the interface

$$m = \rho(\mathbf{u}_{\text{int}} - \mathbf{u}) = k\nabla T / h_{\text{fg}} \tag{8}$$

In the level set formulation the level set function φ is advanced and reinitialized according to the following partial differential relations:

$$\partial_t \varphi = -\mathbf{u}_{\text{int}} \nabla \varphi \tag{9}$$

$$\partial_t \varphi = \frac{\varphi_o(1 - |\nabla\varphi|)}{\sqrt{\varphi_o^2 + h^2}} \tag{10}$$

where φ_o is a solution of Eq. (9). The surface tension force $(-\sigma\kappa\nabla H)$ is incorporated into the momentum equation and implemented in the volumetric form [22], via a step function H ($H = 0$ in the vapor and 1 in the liquid) and κ is the interfacial curvature, which is expressed as

$$\kappa = \nabla[\nabla\varphi / |\nabla\varphi|] \tag{11}$$

$$\kappa = \frac{\varphi_y^2\varphi_{xx} - 2\varphi_x\varphi_y\varphi_{xy} + \varphi_x^2\varphi_{yy}}{(\varphi_x^2 + \varphi_y^2)^{3/2}}, \quad \text{for 2-D} \tag{12}$$

Here the subscripts denote differentiation with respect to φ.

B. Nondimensional Form of the Governing Equations

The nondimensional form of the preceding governing equations was derived using a characteristic length (l_r), velocity (u_r), time (t_r), and temperature (T^*). The definition for each of these terms is shown in Eqs. (13–16). These values were defined in a manner similar to the convention used in the works by Son and Dhir [18] and Selvam and Ponnappan [12]

$$l_r = \sqrt{\frac{\sigma}{g(\rho_l - \rho_v)}} \tag{13}$$

$$u_r = \sqrt{g l_r} \tag{14}$$

$$t_r = l_r / u_r \tag{15}$$

$$T^* = \frac{T - T_{\text{sat}}}{T_w - T_{\text{sat}}} \tag{16}$$

Using these reference values for the baseline gravity condition ($1.0g = 9.8\ \text{m/s}^2$), the Bond and Froude numbers become unity ($Bo = Fr = 1$) with the Weber number equation simplifying to the liquid density divided by the liquid–vapor density difference. For a liquid density much greater than a corresponding vapor density (i.e., $\rho_l \gg \rho_v$), $We \approx 1$. Considering ρ, k, μ, and c_p of liquid and vapor as fixed in each phase, the nondimensional equations (without their subscripts) are expressed as follows:

$$\rho(\partial_t \mathbf{u} + \mathbf{u}\nabla\mathbf{u}) = -\nabla p + \frac{\rho g_y}{Fr^2} - \frac{\kappa\nabla H}{We} + \frac{\nabla\cdot\mu\nabla\mathbf{u} + \nabla\cdot\mu\nabla\mathbf{u}^T}{Re} \tag{17}$$

$$c_{\text{pl}}(\partial_t T + \mathbf{u}\nabla T) = \frac{\nabla\cdot k\nabla T}{Pe} \quad \text{for } H > 0 \tag{18}$$

$$\nabla\cdot\mathbf{u} = \frac{Ja\cdot k\nabla T\cdot\nabla\rho}{Pe\cdot\rho^2} \tag{19}$$

$$\mathbf{u}_{\text{int}} = \mathbf{u} + \frac{Ja\cdot k\cdot\nabla T}{Pe\cdot\rho} \tag{20}$$

The variable g_y is the gravitational force in the y direction. Variation in gravitational forces is accounted for through the Froude number, as seen in Eq. (17). In the studies, the Froude number was varied between 10,000 ($0.0001g$ case) and 0.5 ($2.0g$ case).

C. Boundary Conditions

The boundary conditions for the governing equations are shown in Fig. 2 and also given in the following:

wall boundary condition
at $y = 0$: $u = v = \varphi_y = 0$, $T = T_w$
planes of symmetry:
at $x = 0$: $u = v_x = T_x = \varphi_x = 0$
at $x = x_{\max}$: $u = v_x = T_x = \varphi_x = 0$
top of the computational domain (i.e., free surface)
at $y = y_{\max}$: $u_y = v_y = \varphi_y = 0$, $T = T_{\text{sat}}$

D. Numerical Solution

The governing Eqs. (1–3), (9), and (10) combined together are highly nonlinear. The equations are discretized using the finite difference method on a staggered grid system in which all the variables except pressure are stored at the grid points; pressure alone is stored at the cell center as shown in Fig. 2. The diffusion terms are considered implicitly, and the convection and source terms are considered explicitly in time. For spatial approximations all terms are considered using second-order central differencing. A second-order essentially nonoscillatory (ENO) method described by Chang et al. [23] is applied to the convection terms to prevent numerical oscillations. The pressure and velocity are solved in a sequential manner by the procedure described in the work by Selvam [24]. The discretized equations for momentum, energy, and pressure are symmetric and are solved by the preconditioned conjugate gradient procedure [25] in an iterative manner. The iteration is performed until the average residue for each node is reduced to less than 10^{-9}. This amount of accuracy is needed because of the large difference in densities between the liquid and the vapor phases. After assuming the initial position for the distance functions, the equations are solved sequentially at each time step in the following order:

1) Solve the momentum equations for velocities.
2) Correct the velocity to account for the pressure effect.
3) Solve the pressure equation (i.e., Poisson's equation) to satisfy continuity.

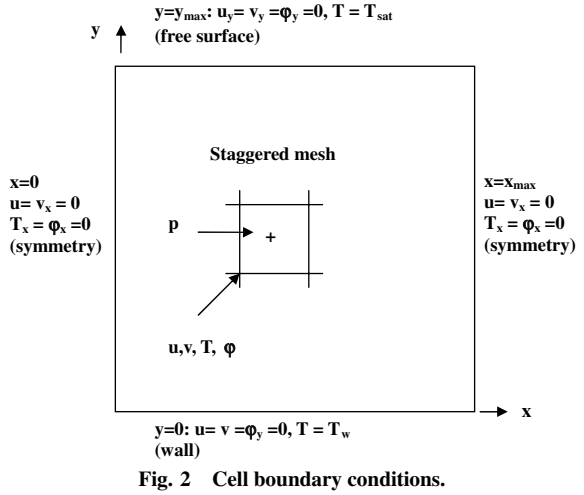

Fig. 2 Cell boundary conditions.

4) Update the velocities to include the new pressure effect.
5) Solve the temperature equation [Eq. (2)].
6) Solve the distance function [Eq. (9)].
7) Reinitialize the distance function defined in Eq. (10) and go to the next time step.

During the computation, time steps were chosen to satisfy the Courant–Fredreichs–Lewy (CFL) condition. This condition is defined mathematically as $\Delta t \leq \min(h/(|u| + |v|))$. This was done because of the explicit treatment of the convection terms and the condition that the numerical results should not change if the time steps are halved.

III. Results and Discussion

FC-72 at 101 kPa has a saturation temperature (Tsat) of 56°C. These conditions are comparable to those in the experimental studies by Lin and Ponnappan [5], which used FC-72 as the working fluid. The present modeling work considers FC-72 at these saturation conditions presented in Table 1. Corresponding numerical reference values used in the model are $l_r = 736.2\ \mu$m, $u_r = 85$ mm/s, $t_r = 8.66$ ms, and $\Delta T_w = 10$°C. Other nondimensional parameters of interest include $Re = 218$, $We = 1.0$, $Pe = 2050$, $Ja = 0.127$, and $\rho_l/\rho_v = 138$. Each of the aforementioned values was used in the present study, with the exception of the density ratio ρ_l/ρ_v. To prevent numerical instability and reduce calculation time, a density ratio of lower magnitude was substituted (i.e., $\rho_l/\rho_v = 20$). Selvam et al. [9] noted that higher density ratios show a trend (in terms of the Nusselt number) similar to lower density ratios; however, the maximum nodal error needed for stable bubble growth is much smaller, thus greatly increasing the overall iteration time. Larger density ratios were not investigated in the present modeling effort.

A. Vapor Bubble Growth

Vapor bubble growth in varying gravitational fields (neglecting bubble merger and droplet impingement) was investigated for comparison to currently accepted theories on vapor bubble growth and fluidic behavior in microgravity. As mentioned previously, Dhir et al. [14] predicted bubble separation diameters of 2.3 mm for $1.0g$ and 209 mm for $0.0001g$ using water under pool boiling conditions. These size predictions for bubble separation diameters are beyond the grid size limits of the model used in the present thin-film study. The size scale selected for the liquid film thickness in the present study corresponds with the size scale for individual droplets and bubble nucleation taking place within a thin film under a liquid spray. Nonetheless, in order to validate the predictive capability of the present model, growth phenomena for a large-domain bubble size was studied and compared qualitatively against the work of Dhir et al. [14]. A $2 \times l_r$ (1.47 mm) domain was used with an initial bubble radius of $1 \times l_r$ (0.74 mm). The discretized grid mesh was 201×201, thus creating individual cells with characteristic lengths of 7.31 μm. A time step of $6 \times 10^{-6} \times t_r$ (52 ns) was used for 16,000 iterations, creating an overall time interval of 832 μs. Figure 3 shows the Nusselt number and maximum velocity whereas Figs. 4 and 5 show the time evolution of the velocity vectors for both 2.0 and $0.0001g$ at times of 438 and 788 μs, respectively. The $1.0g$ case is not shown.

Table 1 Working Fluid Thermophysical Properties and Simulation Parameters

Spray Cooling Parameters	
Parameters	*Value*
P_{sat}	101 kPa
T_{sat}	56°C
T_l	56°C
h_{fg}	76 kJ/kg
c_p	1.046 kJ/kg°C
σ	0.011 N/m
ΔT_w	10°C

As shown in Figs. 3–5, the Nusselt number decreases as the bubble grows and the amount of liquid in contact with the hot wall decreases. At $t = 0.543 \times t_r$ for the $2.0g$ case and $t = 0.820 \times t_r$ for the $1.0g$ case, the Nusselt number spikes and oscillates at an increased amplitude (shown by the latter half of Fig. 3a). This corresponds to the start of vapor bubble departure from the heater surface, which is shown in Fig. 5a as the bottom of the bubble inflects inward at the solid–liquid–vapor interface in preparation for wall separation. As the vapor bubble detaches, the liquid–solid contact area increases allowing for more heat transfer via conduction through the liquid film. The Nusselt number continued to increase as the bubble completely detached from the surface. This feature is notably absent from the $0.0001g$ case where the bubble continues to grow. This growth is similar to that described in Dhir et al. [14], who found that in reduced gravity bubbles tend to grow in oblong spherical shapes and have much larger separation diameters than in $1.0g$. Dhir's work, as well as the results observed using the present comparison study show that the primary effect of reducing gravity is a reduction in the buoyant forces that promote bubble detachment from the heater surface in $1.0g$. This suggests that surface tension and viscosity play a more significant role in microgravity than in $1.0g$.

The microscale study case uses a domain length of $0.4 \times l_r$ (294.5 μm) and an initial bubble radius of $0.2 \times l_r$ (147.2 μm) to reflect the heat transfer occurring at the corners of the die as reported by Pautsch et al. [13]. The corners/edges are where droplet impingement and vapor merger were reported to occur less frequently, thus making nucleate boiling the primary means of heat transfer in this region. A 101×101 grid domain was used for this simulation. The corresponding characteristic length for a single grid was 1.46 μm.

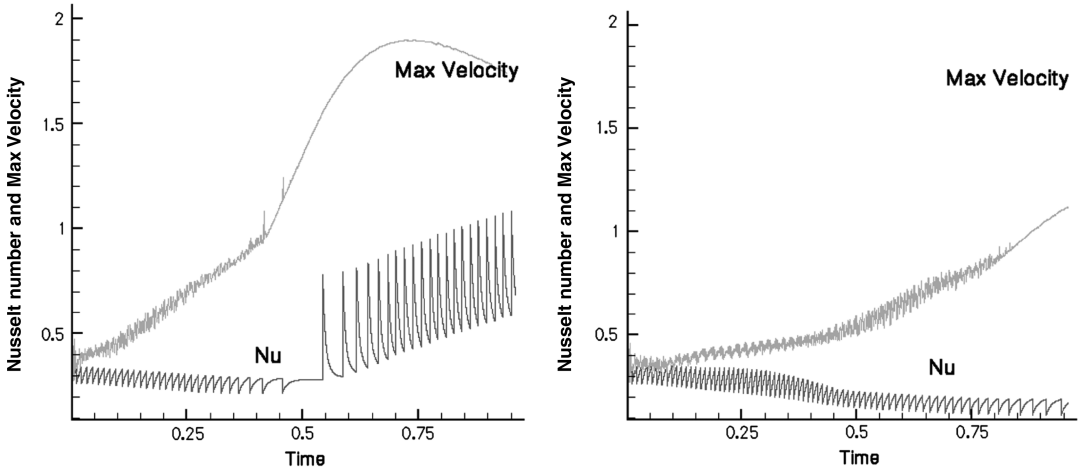

a) Gravitational constant = 2.0g **b) Gravitational constant = 0.0001g**

Fig. 3 Large vapor bubble growth study Nusselt number and maximum velocity as a function of time.

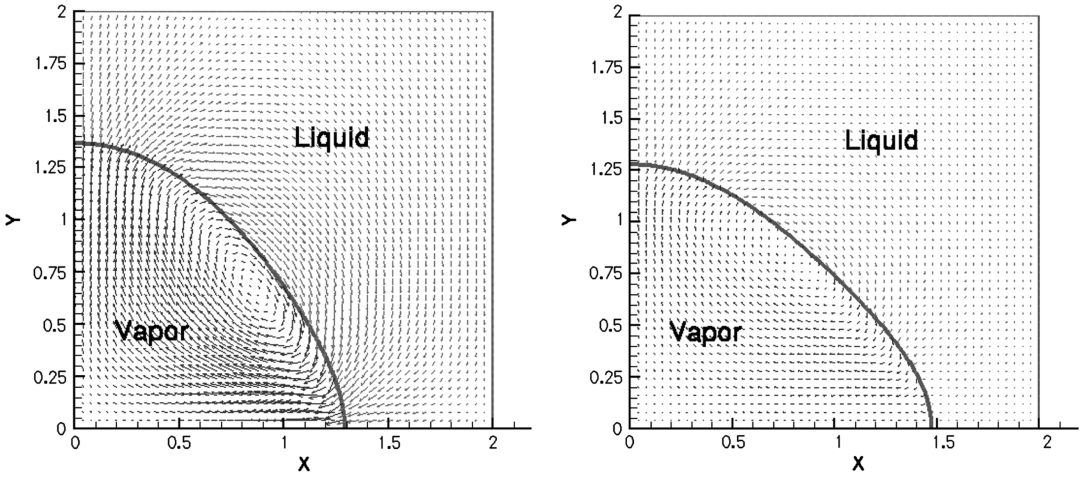

a) Gravitational constant = 2.0g b) Gravitational constant = 0.0001g

Fig. 4 Large vapor bubble growth study liquid–vapor vector diagram snapshots at $t = 438$ μs showing a) gravitational constant = 2.0g, and b) gravitational constant = 0.0001g.

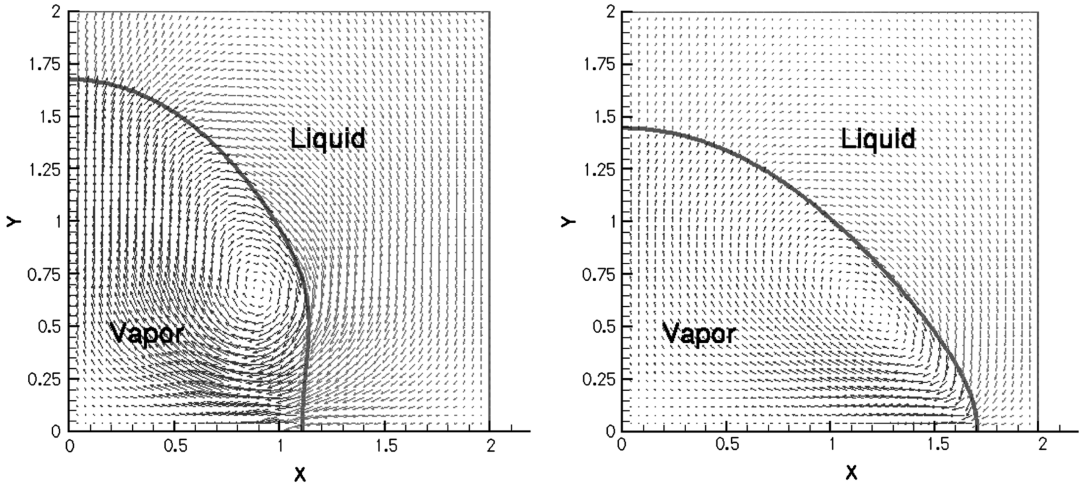

a) Gravitational constant = 2.0g b) Gravitational constant = 0.0001g

Fig. 5 Large vapor bubble growth study liquid–vapor vector diagram snapshots at $t = 788$ μs showing a) gravitational constant = 2.0g, and b) gravitational constant = 0.0001g.

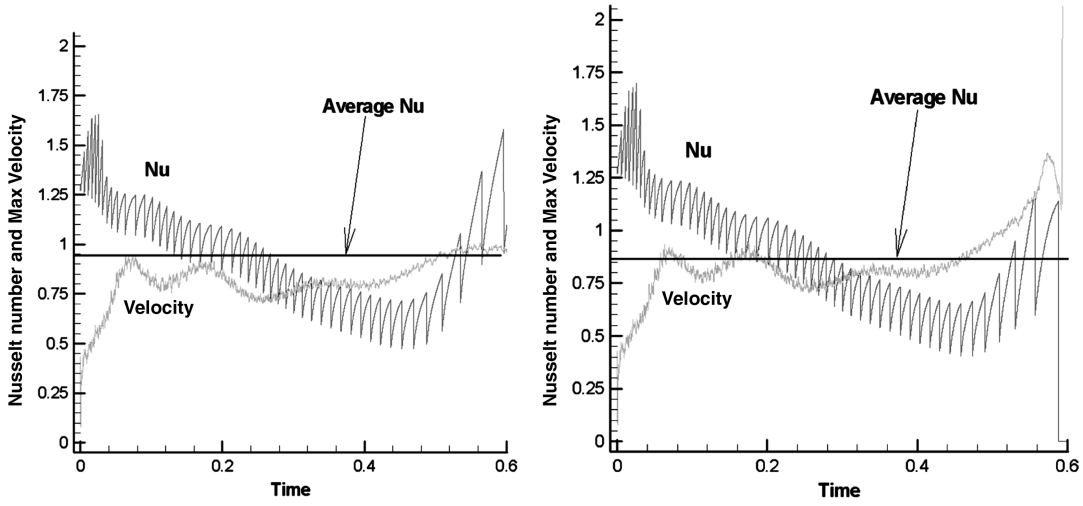

a) Gravitational constant = 1.0g b) Gravitational constant = 0.0001g

Fig. 6 Vapor growth study Nusselt number and maximum velocity as a function of time showing a) gravitational constant = 1.0g, and b) gravitational constant = 0.0001g.

The time step used in the study by Dhir et al. [14] was 2×10^{-5} time units (173 ns), larger than that used by Selvam et al. [9,11]. Selection of the time step for use in the thin-film study was necessitated by the larger domain and relative slow speed of vaporization in the model for $\Delta T_w = 10°\text{C}$ (this still obeyed the CFL condition). Results for the 1.0 and $2.0g$ cases were very similar. Therefore, only the $1.0g$ case is presented for comparison against the $0.0001g$ case. The Nusselt number, time-averaged Nusselt number, and maximum velocity for the microscale study is shown in Fig. 6. In the figure, the plotted velocity profile records the largest velocity within the computational domain at each specified time and is an aid for determining computational stability of a given simulation. Figures 7 and 8 each show vector plots for the liquid and vapor phase velocities at different times.

The growth rate and shapes of the bubbles did not change significantly with gravitational variation. At the time 4.38 ms (Fig. 8), the sizes of the bubbles were $3.75 \times l_r$ by $3.65 \times l_r$ for $2.0g$, $3.70 \times l_r$ by $3.75 \times l_r$ for $1.0g$, and $3.7 \times l_r$ by $3.8 \times l_r$ for $0.0001g$. There is only a slight difference in the bubble aspect ratio between the 2.0 and $1.0g$ cases. In the $2.0g$ case, the bubble grown is slightly taller and narrower than its $1.0g$ counterpart. However, in the 1.0 and $0.0001g$ cases the bubbles are virtually identical. The Nusselt number peaked for all cases at $t = 0.04 \times t_r$ (346 μs), which corresponds with the initial formation of the convective cell created by a liquid phase change at the wall. This is denoted by the velocity vortex near the wall. This vortex is an artifact of initial parameters selected in the model for the starting size of the vapor bubble and the initial velocity condition (velocity was initially set to zero throughout the domain). Once the system has achieved a steady state, such effects will be negligible in the overall heat transferred. The Nusselt number increased sharply at $t = 0.04 \times t_r$ (346 μs) and reflected the onset of convection currents along the heated surface due to the velocity vortex. However, the Nusselt number decreased once the velocities stabilized. Because the maximum Nusselt number for these cases was influenced by the aforementioned initial conditions, comparisons between different gravitational cases will be based on the time-averaged Nusselt number rather than the maximum Nusselt number. The time-averaged Nusselt number values were 0.943, 0.987, and 0.881 for the 2.0, 1.0, and $0.0001g$ cases, respectively. The two mechanisms for heat transfer occurring throughout the simulation are vaporization of the liquid at the solid–liquid–vapor interface along the wall and conduction through the liquid region in contact with the heated wall. The average Nusselt number for the $0.0001g$ case was lower than the 1.0 and $2.0g$ cases because the large bubble created a barrier for the liquid path to the heater surface, thereby limiting the amount of conduction. The time-averaged

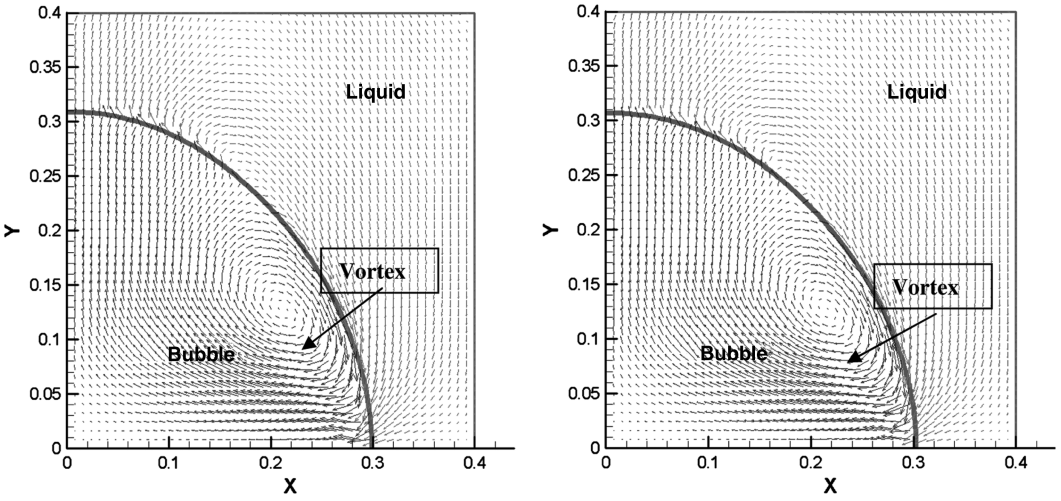

a) Gravitational constant = 1.0g b) Gravitational constant = 0.0001g

Fig. 7 Vapor growth study liquid–vapor vector diagram snapshots at $t = 2.19$ ms showing a) gravitational constant = $1.0g$, and b) gravitational constant = $0.0001g$.

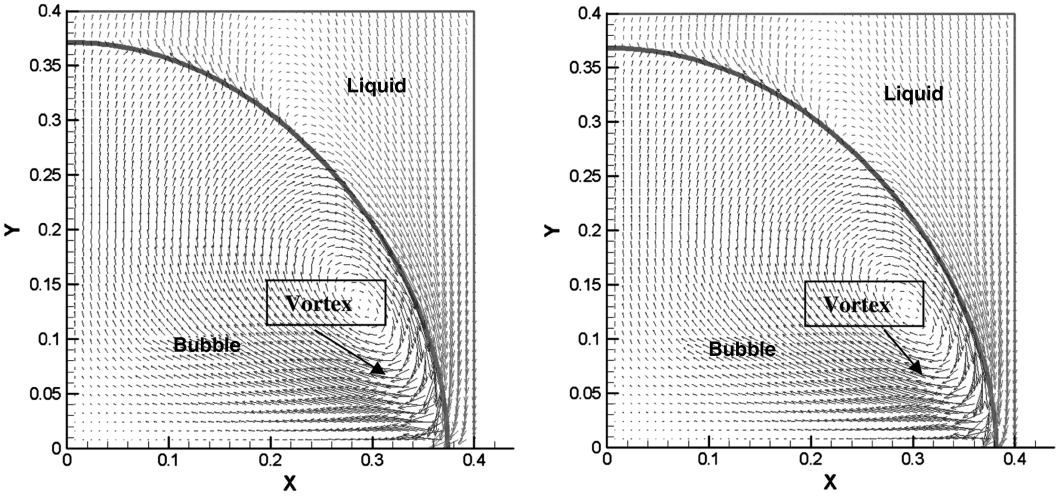

a) Gravitational constant = 1.0g b) Gravitational constant = 0.0001g

Fig. 8 Vapor growth study liquid vapor vector diagram snapshots at $t = 4.38$ ms showing a) gravitational constant = $1.0g$, and b) gravitational constant = $0.0001g$.

Nusselt number for the $2.0g$ case was only slightly lower then the $1.0g$ case. This is due to the $2.0g$ bubble interacting with the upper boundary of the computational domain, which had a free-surface condition. This coupling was not expected before runtime.

Based on the results of the thin liquid film study, it is clearly shown that for a bubble of radius 147.2 μm or less, gravitational variation has little influence on bubble growth and the nondimensional heat transfer coefficient. This is due to the high surface tension effects present in bubbles having a radius of 147.2 μm or less.

The study by Dhir et al. [14] showed that the $1.0g$ case took 0.25 s to grow a bubble to a size of 6.2 mm (critical diameter). For the microgravity case, bubble growth to the critical diameter (209 mm) and departure from the heater surface spanned 135 s. This implies that in order to achieve bubble departure for the microgravity case, an increased amount of computational time and space would be necessary due to the reduced buoyancy effects. Because the spray cooling film thickness is much smaller than the previously reported microgravity separation diameter that occurs during pool boiling, nucleate boiling alone is incapable of capturing the actual physical process. Bubble merger with a vapor region must also be considered for thin-film modeling.

B. Thin-Film Bubble–Vapor Merger

For the thin-film case, a bubble of radius 66.3 μm was positioned at the origin of a liquid film, which was $0.1 \times l_r$ (73.6 μm) thick. This bubble was grown computationally until it merged with the vapor layer above it. The computational domain used was $0.4 \times l_r \times 0.4 \times l_r$ (294.4 μm). This was discretized into a 101×101 grid, which created uniform square grids with a side length of 2.92 μm. A time step of $5 \times 10^{-6} \times t_r$ (43.3 ns) was used for 40,000 iterations, giving a total time interval of 1.73 ms. Because of the fact that the velocity vector plots showed similar behavior between the 2.0 and $1.0g$ cases, results from the $2.0g$ cases are not explicitly detailed in the present work. The Nusselt number and time-averaged Nusselt number as well as the maximum velocity in the computational domain are shown in Fig. 9. Vector plots for both gravitational cases (0.0001 and $1.0g$) at $t = 0.032 \times t_r$ and $t = 0.064 \times t_r$ are shown in Figs. 10 and 11.

The time-averaged Nusselt number for cases 0.0001, 1.0, and $2.0g$ (not shown) were 10.302, 10.303, and 10.307, respectively. The maximum variation between these values was 0.0004%. The peak Nusselt number occurred for all cases when the vapor–bubble merged with the vapor layer above it. For the $1.0g$ case, this occurred at $t = 0.047585 \times t_r$ (412 μs) with Nu = 20.733. For the $0.0001g$ case, this occurred at $t = 0.047380 \times t_r$ (410 μs) and had Nu= 20.711. In the $2.0g$ case (not shown) the vapor–bubble merger occurred at $t = 0.047000 \times t_r$ (407 μs) with Nu = 20.661. As with the time-averaged values, these cases have a variation much less than 1%. In each of the cases, the peak in the Nusselt number corresponds closely with the peak in maximum velocity for each case. As noted previously in the bubble growth case, this occurred when the vapor

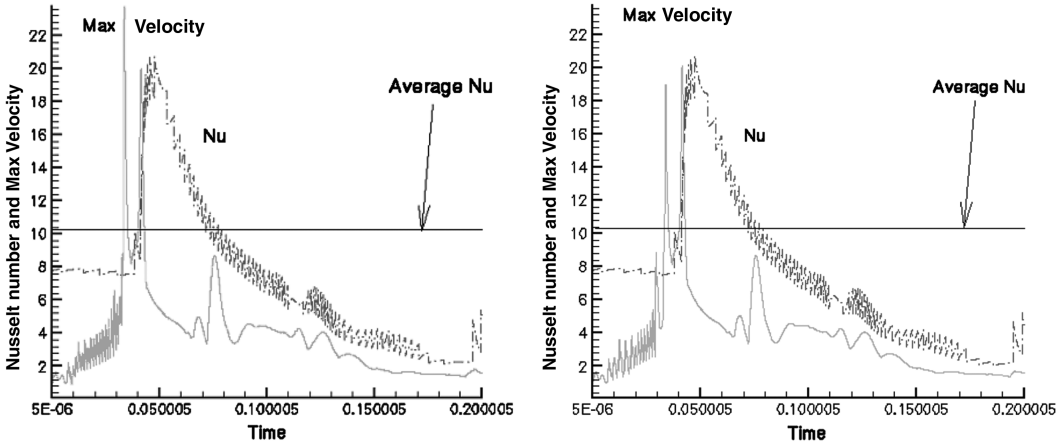

a) Gravitational constant = 1.0g b) Gravitational constant = 0.0001g

Fig. 9 Thin-film bubble–vapor merger study Nusselt number and maximum velocity as a function of time showing a) gravitational constant = $1.0g$, and b) gravitational constant = $0.0001g$.

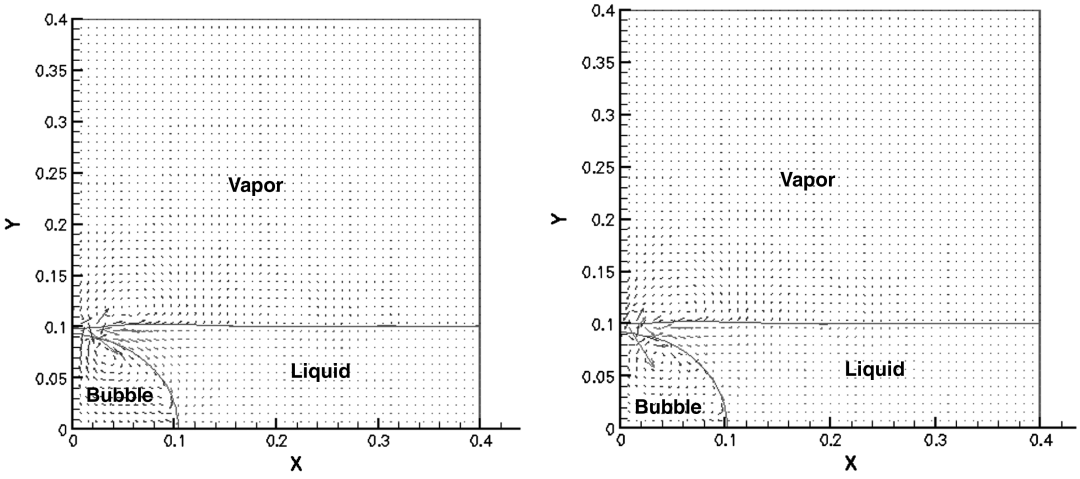

a) Gravitational constant = 1.0g b) Gravitational constant = 0.0001g

Fig. 10 Thin-film bubble–vapor merger study liquid–vapor vector diagram snapshots at $t = 273$ μs showing a) gravitational constant = $1.0g$, and b) gravitational constant = $0.0001g$.

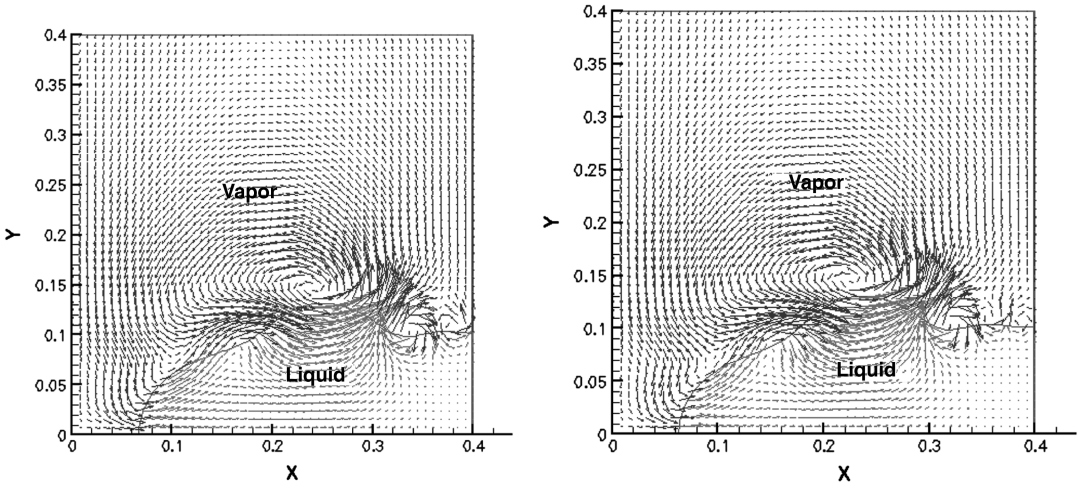

a) Gravitational constant = 1.0g b) Gravitational constant = 0.0001g

Fig. 11 Thin-film bubble–vapor merger study liquid–vapor vector diagram snapshots at $t = 273$ μs showing a) gravitational constant = 1.0g, and b) gravitational constant = 0.0001g.

bubble merged with the vapor at the liquid–vapor interface. Therefore, one may conclude that the peak in the Nusselt number is due to the increased movement of the system, which allowed liquid replenishment of the heated wall in locations previously occupied by superheated vapor. Selvam et al. [9] found similar results for a gravitational constant of 1.0g.

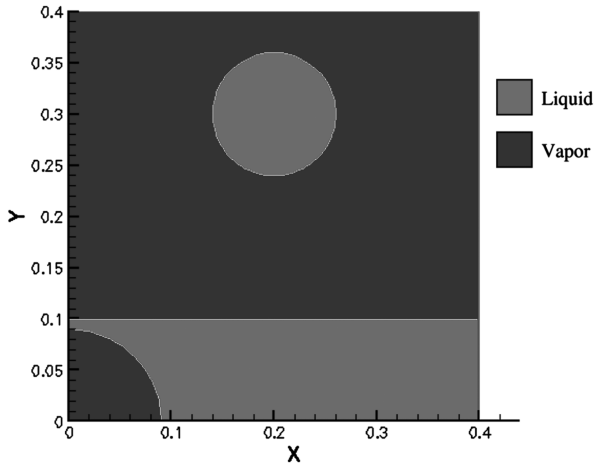

Fig. 12 Droplet impingement model configuration schematic.

C. Droplet Impingement on a Growing Bubble

For the droplet impingement case, simulation conditions similar to that used in the bubble–vapor merger study were applied. The primary difference was that a droplet was added to the solution domain. The droplet had a radius of $0.06 \times l_r$ (44.2 μm) and was placed with its center $0.2 \times l_r$ above the film and $0.2 \times l_r$ to the right of the y axis (as shown in Fig. 12). The y axis is coincident with the bubble center. The droplet had an initial dimensionless velocity of $20 \times u_r$ downward (i.e., 1.7 m/s). In the study by Selvam and Ponnappan [12], a dimensionless unit velocity of $30 \times u_r$ (2.56 m/s) was used to more closely resemble the experimental conditions in the work by Baysinger et al. [26]. Although the previous droplet impingement studies by Selvam and Ponnappan [12] used a 201 × 201 mesh in the solution domain, the present study used a 101 × 101 mesh to attain computational results in a time efficient manner. This meant that a lower droplet velocity had to be used to avoid numerical instabilities. Because of similarities between the 2.0 and 1.0g cases, results presented are only for the 1.0 and 0.0001g cases. Figure 13 shows the Nusselt number and maximum velocities as a function of time and gravitational reference frame. Figures 14 and 15 show the liquid/vapor velocity vector field at times $t = 0.1055 \times t_r$ and $t = 0.1583 \times t_r$, respectively.

Results from the droplet impingement model showed two local Nusselt number maxima for each of the cases with the local Nusselt number maxima occurring at similar times between varying gravity conditions. The first Nusselt number maximum for each case occurs

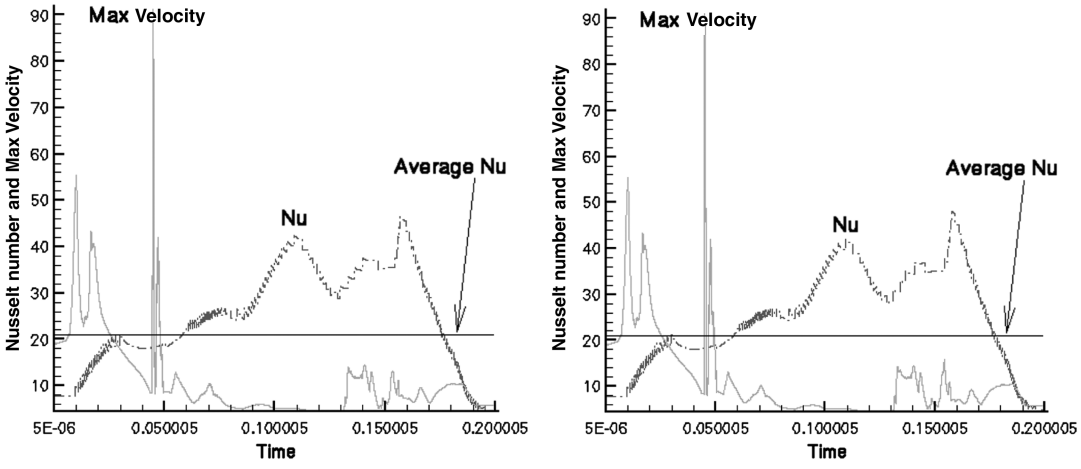

a) Gravitational constant = 1.0g b) Gravitational constant = 0.0001g

Fig. 13 Droplet impingement on liquid film with bubble growth study Nusselt number and maximum velocity as a function of time showing a) gravitational constant = 1.0g, and b) gravitational constant = 0.0001g.

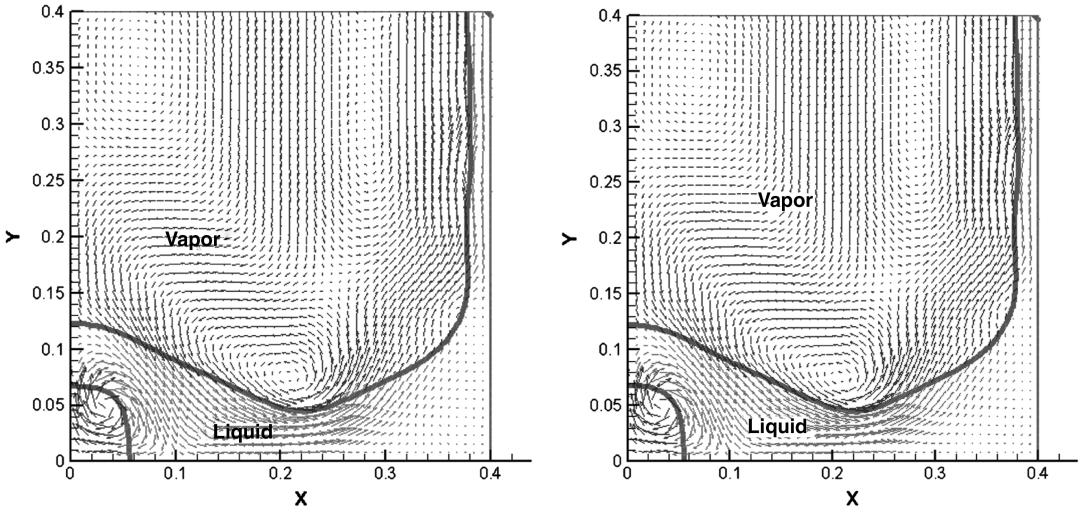

a) Gravitational constant = 1.0g b) Gravitational constant = 0.0001g

Fig. 14 Droplet impingement on liquid film with bubble growth study liquid–vapor vector diagram snapshots at $t = 910$ μs showing a) gravitational constant = 1.0g, and b) gravitational constant = 0.0001g.

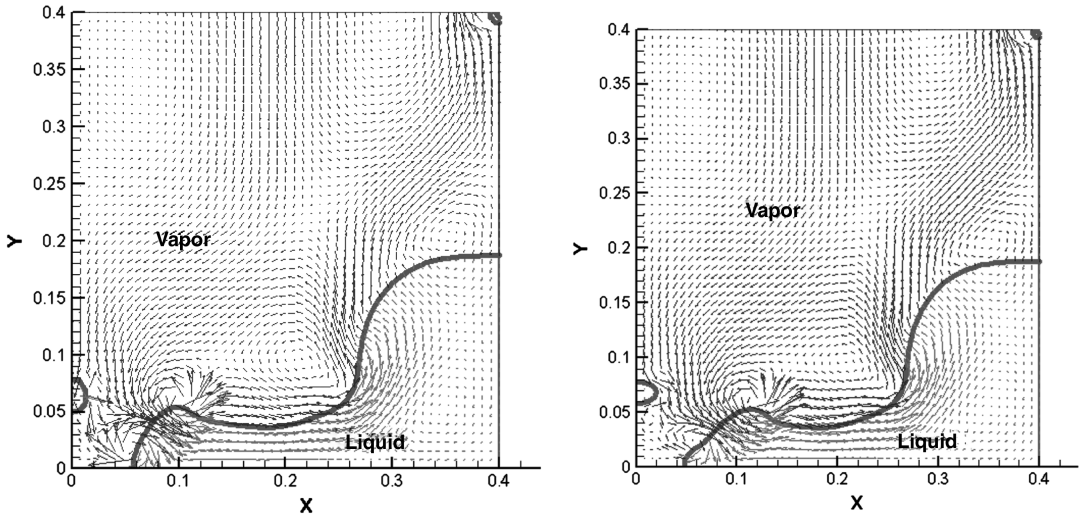

a) Gravitational constant = 1.0g b) Gravitational constant = 0.0001g

Fig. 15 Droplet impingement on liquid film with bubble growth study liquid–vapor vector diagram snapshots at $t = 1.37$ ms showing a) gravitational constant = 1.0g, and b) gravitational constant = 0.0001g.

when the cooled droplet displaces some of the bubble's vapor along the heated wall (shown in Fig. 14), thus causing transient conductive heat exchange. For the 1.0g case, the initial peak occurs at $0.109 \times t_r$ (0.94 ms) with Nu = 42.0. For the 2.0g case, the first peak occurs at $0.108 \times t_r$ (0.94 ms) and also has Nu = 42.0. For the 0.0001g case, the initial peak is at $0.106 \times t_r$ (0.92 ms) and has Nu = 41.1. The second peak in the Nusselt number occurs when the cooled droplet, now completely merged with the liquid film, experiences a secondary contact with the hot wall, creating a large thermal gradient that results in higher heat flux at the heater surface. The 1.0 and 0.0001g cases are shown in Fig. 15. For the 1.0g case, this secondary contact gave Nu = 48.1 at $1.58 \times t_r$ (1.37 ms). For the 2.0g case (not shown) Nu = 47.9 occurred at $0.156 \times t_r$ (1.35 ms). For the 0.0001g case the secondary peak occurred at $1.58 \times t_r$ (1.37 ms) with Nu = 48.1. This suggests that higher heat fluxes can be achieved when cooler liquid contacts the hot wall directly as opposed to steadily conducting through the liquid film to the free surface that has lower temperature due to droplet impingement.

IV. Discussion

Comparison of the study cases for microgravity and macrogravity on a bubble of radius 0.74 mm showed that the model contained the ability to capture differences inherent to the bubble growth process (and ultimately the bubble size) verifying the model's capability to simulate the differences in bubble growth phenomena in variable gravitational environments. Given the successful validation of the model, a better understanding of the physical phenomena captured in the thin-film modeling effort can be attained through review of each of the study cases investigated.

In the present studies, the Nusselt number was reported as a function of the gravitational effects and the respective study case's flow and nucleate boiling scenarios. Heat transfer (i.e., $\dot{q}''$) was not explicitly investigated and reported. Thus, determinations regarding the effect of gravity on fluid flow and nucleate boiling in a thin film undergoing spray cooling were limited to those that could be discerned via the Nusselt number. Complementary heat transfer effects due to temperature gradients in the film have not been captured.

Table 2 gives a comprehensive listing of the gravitational constant, time-averaged Nusselt number, peak velocity value, and corresponding time of occurrence as well as the peak Nusselt number values and their corresponding time of occurrence for each of the study cases modeled. In the microscale film layer with small bubble growth study, variation in the gravitational constant was shown to have little effect upon bubble growth and heat transfer. However, the

Table 2 Summary of simulation studies

Simulation case	Gravitational constant, g	Time-averaged Nusselt number, $\overline{\mathrm{Nu}}$	Peak velocity values		Peak Nusselt number values[a]	
			Velocity, m/s	Time, m/s	Nusselt number	Time
Small vapor bubble growth	2.0	0.943	0.086	4.877	——	——
	1.0	0.987	0.082	4.919	1.62	182 μs
	0.0001	0.881	0.116	4.967	1.697	220 μs
Large vapor bubble growth	2.0	0.405	0.161	6.400	1.034	8.23 ms
	1.0	0.272	0.142	7.676	0.807	8.16 ms
	0.0001	0.222	0.032	0.020	0.350	0.471 ms
Thin-film bubble–vapor merger	2.0	10.307	1.990	0.288	20.661	407 μs
	1.0	10.303	2.021	0.291	20.733	412 μs
	0.0001	10.302	1.709	0.359	20.711	410 μs
Droplet impingement on a thin-film with a growing bubble			*Initial contact*			
	2.0	21.111	8.246	0.388	42.0	0.94 ms
	1.0	21.114	8.118	0.391	42.0	0.94 ms
	0.0001	21.114	8.118	0.391	41.1	0.92 ms
			Secondary contact			
	2.0	21.111	1.236	1.218	47.9	1.35 ms
	1.0	21.114	1.231	1.215	48.1	1.37 ms
	0.0001	21.114	1.342	1.336	48.1	1.37 ms

[a]Based on liquid–vapor vector field

Nusselt number increased as the bubble completely detached from the surface. In the thin-film bubble–vapor merger study, the average Nusselt number over the computational time for the simulation (1.73 ms) was approximately the same for each of the gravitational cases. However, each of the gravitational cases showed a peak in the Nusselt number upon the vapor bubble merging with the vapor layer above the thin film. Furthermore, this peak corresponded with the peak in the maximum velocity. In the droplet impingement on a growing bubble study, two local maxima were shown to occur in each of the gravitational cases: when the cooled droplet displaces part of the bubble's vapor along the heated wall upon impingement and during secondary contact of the newly replenished liquid with the heated wall. Nusselt number values for the maxima associated with the secondary contact of the newly replenished liquid (approximately 48.0) were greater than those resulting from bubble–vapor displacement for each of the gravitational cases.

Spray cooling is considered a multiphase convective process. The Nusselt number, which is the nondimensional heat transfer coefficient used for convective processes, is a function of the convection coefficient, the heat exchange surface's characteristic length scale, and the working fluid's thermal conductivity. The convection coefficient is a function of the thermophysical properties of the fluid and the flow scenario. Given the inclusion of the convection coefficient in the Nusselt number definition and the fact that the solution domain and working fluid test conditions were the same in each study for all the gravitational cases, differences in the reported Nusselt number for each of the study cases may be considered a function of the flow scenario in the models. In each of the studies, the increase in the peak Nusselt number occurs at times in the simulation where the film experiences bulk fluid motion either due to bubble detachment (initiated by full bubble growth or droplet impingement) and/or bubble–vapor merger. This is in agreement with the determinations of Pautsch and Shedd [6]. Also, although the Nusselt number peaks observed in the study cases are associated with bulk fluid motion in the thin film, this motion is coupled to nucleate boiling phenomena. In each case, the Nusselt number peaks occurred when the newly replenished liquid advanced onto heater wall locations previously occupied by vapor. Thus, increased bulk fluid motion in the thin film may be considered a phenomenon that promotes better heat transfer in spray cooling processes via transient conduction resulting from the bubble detachment/liquid advancement sequence. In addition, the lack of Nusselt number dependence upon variation in the gravitational constant suggests that the mechanism of transient conduction has negligible dependence upon gravity.

V. Conclusions

Upon completion of our study, the following conclusions were drawn:

1) For the $0.2 \times l_r$ domain vapor bubble growth case, it was shown that gravity does not play a significant role in heat transfer. The maximum variation between gravity cases (1.0 and $0.0001g$) provided a difference in of 10%. It was also shown that the convective cell and vaporization of the liquid were the primary means of heat transfer. Neither of these phenomena was seen to exhibit significant differences under varying gravitational reference frames.

2) For the case of the large-scale vapor bubble with growth, gravity dependence was observed in the model. In this case the primary means of heat transfer was vaporization along the heater surface at the liquid–bubble interface as well as transient conduction due to localized bulk fluid motion. This motion was primarily due to bubble departure. Thus heat transfer for large-scale vapor bubble growth is dependent on both buoyancy and gravitational forces.

3) For the bubble to liquid–vapor interface merger case, the maximum Nusselt number occurred due to transient conduction caused by the movement of the bubble when bursting. This allowed cooler liquid to come into contact with the heater surface, thereby increasing the thermal gradient at the wall. A maximum variation of 0.3% in the Nusselt number was observed. On the length scale considered, surface tension as opposed to gravitational forces had the dominant effect upon fluid motion and heat transfer.

4) In the droplet impingement case, the heat transfer was not affected significantly by gravity. The factors that provided an

increase in heat transfer compared with the bubble merger case were a result of a relatively larger amount of thermal mass at the liquid–vapor interface contributed by the droplet. The perturbation through the liquid film initiated during droplet contact with the liquid–vapor interface allowed for a larger amount of liquid motion than in the vapor bubble to liquid–vapor interface merger case. In addition, the localized cooling effect created by the droplet provided a larger thermal gradient between the liquid film and the heater surface. This resulted in greater heat transfer, where the Nusselt number varied only 2% between gravitational constants.

5) The bubble growth and vapor merger and droplet impingement modeling studies are part of the spray cooling phenomena. From the study we could conclude that the gravitational variation has little effect on heat transfer.

Acknowledgments

This work was made possible by phase II SBIR grant number NNG06CA07C from NASA Goddard Space Center, Eric Silk contract coordinator, funded through PELS, LLC and the University of Arkansas, Fayetteville. The work was performed at the Computational Mechanics Laboratory at the University of Arkansas, Fayetteville.

References

[1] Cabrera, E., and Gonzalez, J. E., "Heat Flux Correlation for Spray Cooling in the Nucleate Boiling Regime," *Experimental Heat Transfer*, Vol. 16, No. 1, 2003, pp. 19–44. doi:10.1080/08916150303750

[2] Mudawar, I., "Assessment of High Heat-Flux Thermal Management Schemes," *IEEE Transactions on Components and Packaging Technologies*, Vol. 24, No. 2, 2001, pp. 122–141. doi:10.1109/6144.926375

[3] Yang, J., Chow, L. C., and Pais, M. R., "Nucleate Boiling Heat Transfer in Spray Cooling," *Journal of Heat Transfer*, Vol. 118, No. 3, 1996, pp. 668–671. doi:10.1115/1.2822684

[4] Chow, L. C., Sehmbey, M. S., and Pais, M. R., "High Heat Flux Spray Cooling," *Annual Review of Heat Transfer*, Vol. 8, No. 8, 1997, pp. 291–318.

[5] Lin, L., and Ponnappan, R., "Heat Transfer Characteristics of Spray Cooling in a Closed Loop," *International Journal of Heat Mass Transfer*, Vol. 46, No. 20, 2003, pp. 3737–3746.

[6] Pautsch, A. G., and Shedd, T. A., "Spray Impingement Cooling with Single- and Multiple-Nozzle Arrays Part 1: Heat Transfer Data Using FC-72," *International Journal of Heat and Mass Transfer*, Vol. 48, No. 15, 2005, pp. 3167–3175. doi:10.1016/j.ijheatmasstransfer.2005.02.012

[7] Rowden, B. L., Selvam, R. P., and Silk, E. A., "Spray Cooling Development Effort for Microgravity Environments," *Proceedings: Space Technology and Applications International Forum (STAIF 2006), Conference on Thermophysics in Microgravity*, edited by M. S. El-Genk, Vol. 813, American Inst. of Physics, Melville, NY, Feb. 2006, pp. 134–144.

[8] Selvam, R. P., Lin, L., and Ponnappan, R., "Computational Modeling of Spray Cooling: Current Status and Future Challenges," *Proceedings: Space Technology and Applications International Forum (STAIF 2005), Conference on Thermophysics in Microgravity*, edited by M. S. El-Genk, Vol. 746, American Inst. of Physics, Melville, NY, Feb. 2005, pp. 56–63.

[9] Selvam, R. P., Lin, L., and Ponnappan, R., "Direct Simulation of Spray Cooling: Effect of Vapor Bubble Growth and Liquid Droplet Impact on Heat Transfer," *International Journal of Heat and Mass Transfer*, Vol. 49, Nos. 23–24, 2006, pp. 4265–4278. doi:10.1016/j.ijheatmasstransfer.2006.05.009

[10] Selvam, R. P., Baskara, S., Balda, J. C., Barlow, F., and Elshabini, A., "Computer Modeling of Liquid Droplet Impact on Heat Transfer During Spray Cooling," *ASME Summer Heat Transfer Conference*, American Society of Mechanical Engineers, Paper HT2005-72569, July 2005.

[11] Selvam, R. P., Sarkar, M., and Ponnappan, R., "Modeling of Spray Cooling: Effect of Droplet Velocity and Liquid to Vapor Density Ratio on Heat Transfer," *TFAWS 2005: 16th Annual Thermal & Fluids Analysis Workshop*, NASA, Aug. 2005.

[12] Selvam, R. P., and Ponnappan, R., "Numerical Modeling of Nucleation Boiling in Thin Film and Effect of Droplet Impact," *TFAWS 2004: 15th Annual Thermal & Fluids Analysis Workshop*, NASA, Sept. 2004.

[13] Pautsch, A. G., Shedd, T. A., and Nellis, G. F., "Thickness Measurements of the Thin Film in Spray Evaporative Cooling," *Proceedings of the Ninth Intersociety Conference on Thermal and Thermomechanical Phenomena (ITHERM 2004)*, Institute of Electrical and Electronics Engineers, Piscataway, NJ, June 2004, pp. 70–76.

[14] Dhir, V. K., Qiu, D. M., Ramanujapu, N., and Hasan, M. M., "Investigation of Nucleate Boiling Mechanisms Under Microgravity Conditions," *Proceedings of the Fourth Microgravity Fluid Physics and Transport Phenomena Conference*, NASA John H. Glenn Research Center at Lewis Field, Cleveland, OH, March 1999, pp. 435–440.

[15] Qiu, D. M., and Dhir, V. K., "Single-Bubble Dynamics During Pool Boiling Under Low Gravity Conditions," *Journal of Thermophysics and Heat Transfer*, Vol. 16, No. 3, 2002, pp. 336–345. doi:10.2514/2.6710

[16] Hunnell, C. A., Kuhlman, J. M., and Gray, D. D., "Spray Cooling in Terrestrial and Simulated Reduced Gravity," *Proceedings: Space Technology and Applications International Forum (STAIF 2006), Conference on Thermophysics and Applications in Microgravity*, edited by M. S. El-Genk, Vol. 813, American Inst. of Physics, Melville, NY, Feb. 2006, pp. 126–133.

[17] Sussman, M., Smereka, P., and Osher, S., "A Level Set Approach for Computing Solutions to Incompressible Two-Phase Flow," *Journal of Computational Physics*, Vol. 114, No. 1, 1994, pp. 146–159. doi:10.1006/jcph.1994.1155

[18] Son, G., and Dhir, V. K., "Numerical Simulation of Film Boiling Near Critical Pressures with a Level Set Method," *Journal of Heat Transfer*, Vol. 120, No. 1, 1998, pp. 183–192. doi:10.1115/1.2830042

[19] Son, G., Ramanujapu, N., and Dhir, V. K., "Numerical Simulation of Bubble Merger Process on a Single Nucleation Site During Pool Nucleate Boiling," *Journal of Heat Transfer*, Vol. 124, No. 1, 2002, pp. 51–62. doi:10.1115/1.1420713

[20] Sethian, J. A., *Level Set Methods and Fast Marching Methods: Evolving Interfaces in Computational Geometry, Fluid Mechanics, Computer Vision and Materials Science*, Cambridge Univ. Press, Cambridge, UK, 1999.

[21] Osher, S., and Fedkiw, R., *Level Set Methods and Dynamic Implicit Surfaces*, Applied Mathematical Sciences, Springer–Verlag, New York, Vol. 153, 2003.

[22] Brackbill, J. U., Kothe, D. B., and Zamach, C., "A Continuum Method for Modeling Surface Tension," *Journal of Computational Physics*, Vol. 100, No. 2, 1992, pp. 335–354. doi:10.1016/0021-9991(92)90240-Y

[23] Chang, Y. C., Hou, T. Y., Merriman, B., and Osher, S., "A Level Set Formulation of Eulerian Interface Capturing Methods for Incompressible Fluid Flows," *Journal of Computational Physics*, Vol. 124, No. 2, 1996, pp. 449–464. doi:10.1006/jcph.1996.0072

[24] Selvam, R. P., "Computation of Pressures on Texas Tech Building Using Large Eddy Simulation," *Journal of Wind Engineering and Industrial Aerodynamics*, Vols. 67 and 68, 1997, pp. 647–657. doi:10.1016/S0167-6105(97)00107-4

[25] Ferziger, J. H., and Peric, M., *Computational Methods for Fluid Dynamics*, Springer–Verlag, New York, 2002.

[26] Baysinger, K. M., Yerkes, K., Michalak, T., Harris, R., and McQuillen, J., "Design of a Microgravity Spray Cooling Experiment," *42nd AIAA Aerospace Sciences Conference and Exhibit*, Reno, NV, Jan. 2004.